Transonic liquid bells

P. Brunet
Laboratoire de Physique et Mécanique des Milieux Hétérogènes—UMR 7636 CNRS Ecole Supérieure de Physique et Chimie Industrielles 10, rue Vauquelin, 75231 Paris Cedex 05, France

C. Clanet
Institut de Recherche sur les Phénomènes Hors Equilibre—UMR 6594, Technopôle de Château Gombert, 49 rue Frédéric Joliot-Curie, BP146, 13384 Marseille Cedex 13, France

L. Limat
Laboratoire de Physique et Mécanique des Milieux Hétérogènes—UMR 7636 CNRS Ecole Supérieure de Physique et Chimie Industrielles 10, rue Vauquelin, 75231 Paris Cedex 05, France and Fédération de Recherche Matière et Système Complexes, Université Paris 7, FR 2438 CNRS, 2 place Jussieu, 75251 Paris Cedex 05, France

(Received 31 July 2003; accepted 18 March 2004; published online 4 June 2004)

The shape of a liquid bell resulting from the overflow of a viscous liquid out of a circular dish is investigated experimentally and theoretically. The main property of this bell is its ability to sustain the presence of a ''transonic point,'' where the liquid velocity equals the speed of antisymmetric—or sinuous—surface waves. Their shape and properties are thus rather different from usual ''hypersonic'' water bells. We first show that the bell shape can be calculated very accurately, starting from the sonic point. We then demonstrate the extreme sensitivity of the shape of these bells to the difference of pressure across the interface, making them a perfect barometer. Finally, we discuss the oscillations of the bell which occur close to the bursting limit. © *2004 American Institute of Physics.* [DOI: 10.1063/1.1738650]

I. INTRODUCTION

Water bells appear when a cylindrical liquid jet impacts on a solid disk of similar diameter. An example is presented in Fig. 1. The shape of these bells is a famous problem that goes back to the pioneering experimental work of Savart[1] and theoretical work of Boussinesq,[2] who has shown that in the low-gravity regime, the shape of opened bells reduces to a catenary. These objects are usually observed by impacting a disk with a jet,[1] or by extruding liquid across a thin circular slot.[3] A complete study combining experiments as well as analytical calculations was performed by Taylor,[4] comparing direct measurements of the shape with exact calculations. These solutions of the bell shape problem were numerically studied by Lance and Perry.[5] Very recently, the study of liquid bells has shown a revival. Buckingham and Bush[6] reported the possible existence of polyhedral shapes in the impingement problem with a viscous liquid jet. Also, Clanet[7] has recently discussed the stability and oscillations of the bells.

Such studies are not only motivated by the aesthetic and fundamental interest. Liquid bell formation and rupture is observed[8,9] and used in a variety of atomization devices, especially in engines where liquid fuel burns as drops.[10] Finally, the study of liquid bell stability is connected to that of falling planar liquid curtains, such as those involved in coating techniques[11,12] or in paper making.[13] Such liquid curtains are usually formed below a rectangular slot or in more complicated devices just below an inclined rectilinear wedge. Their stability still remains a disputed problem,[11,14–16] because of the nonuniformity of the velocity field that complicates the analysis.

To be more precise, all available theoretical studies of curtain stability basically involve the comparison between two velocities: the fluid velocity U and a critical velocity that reads

$$U_s = \left(\frac{2\sigma}{\rho E}\right)^{1/2}, \tag{1}$$

where E is the local thickness, σ is the surface tension, and ρ is the density. For a millimetric thick sheet formed with a silicone oil ($\rho \approx 980\ \mathrm{kg\,m^{-3}}$, $\sigma \approx 0.02\ \mathrm{kg\,s^{-2}}$), U_s is of the order of $20\ \mathrm{cm\,s^{-1}}$. This velocity can receive two interpretations. On one hand, it is the velocity of sinuous waves propagating on the sheet (i.e., waves conserving the thickness) and more generally on any liquid sheet of constant thickness E.[4] It is also the velocity at which the boundaries of a hole drilled across the inviscid sheet recedes under the combined actions of surface tension and inertia.[4,17]

These interpretations imply that ''usual'' water-bells are supersonic: indeed, these bells form when the velocity of the jet overcomes the retraction speed of the rim, a condition which implies that the velocity in the liquid sheet is always larger than the speed of antisymmetrical waves.

Depending on the authors, and on the specific geometry involved, the instability of a liquid curtain is usually attributed to the growth of sinuous waves that are able to propagate upstream,[14,15] or to the growth of a hole and again especially its ability to grow upstream.[18] In both cases, one is

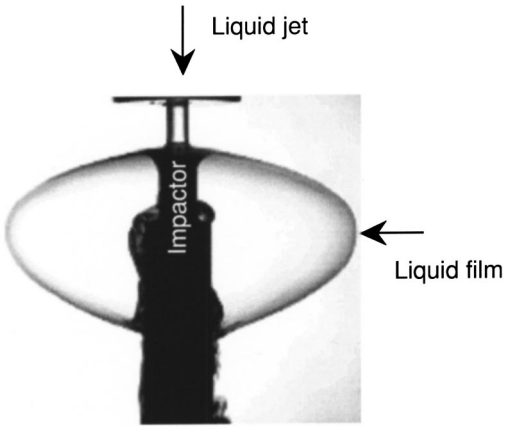

FIG. 1. Example of water bell obtained through the impact of a 3 mm jet diameter on a 6 mm circular impactor.

led to distinguish two regions in a curtain accelerated by gravity: an upstream unstable region in which $U<U_s$ and a downstream stable region for which $U>U_s$. Using the analogy between sound waves and sinuous waves, the upstream region is often called a ''subsonic'' region, and the downstream region a ''supersonic'' region. The line separating both regions being called ''transonic.''

The distinction between these two regions can also be expressed in terms of a ''Mach number,'' which is here the Weber number

$$\mathrm{We}\equiv\left(\frac{U}{U_s}\right)^2=\frac{\rho E U^2}{2\sigma}. \tag{2}$$

Of course, the coexistence of both regimes is avoided if the fluid is injected at the top of the curtain with a velocity higher than $\sqrt{2\sigma/(\rho E)}$. This is the case of classical water bells, which can only form if $U/U_s>1$.[7] Typically, impact velocities for classical water bells are of the order of the meter per second and the whole bell is supersonic.

We underline that the structure of the flow in a falling curtain (the liquid flows from the subsonic to the supersonic region) is exactly the inverse of what happens in an axisymmetrical sheet obtained by impacting a jet on an obstacle. Such an axisymmetrical sheet is presented in Fig. 2. In this latter case, since the velocity is constant in the sheet and the thickness decreases with the distance from the impact, the liquid flows from the supersonic to the subsonic region. In practice, this axisymmetrical liquid sheet is observed to disintegrate at the sonic point[9] (development of an atomization front). The situation is more complicated for a falling curtain, because the unstable region stays upstream: the curtain should break as a whole, its stability becoming a global problem.

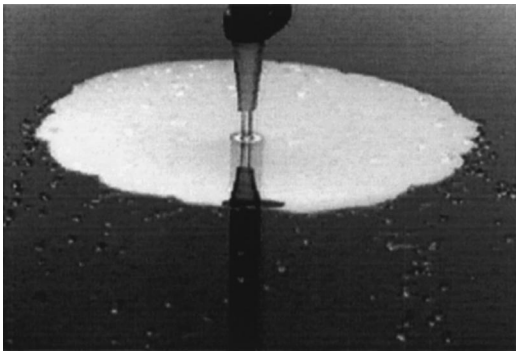

FIG. 2. Example of axisymmetrical water sheet desintegrating at the sonic point.

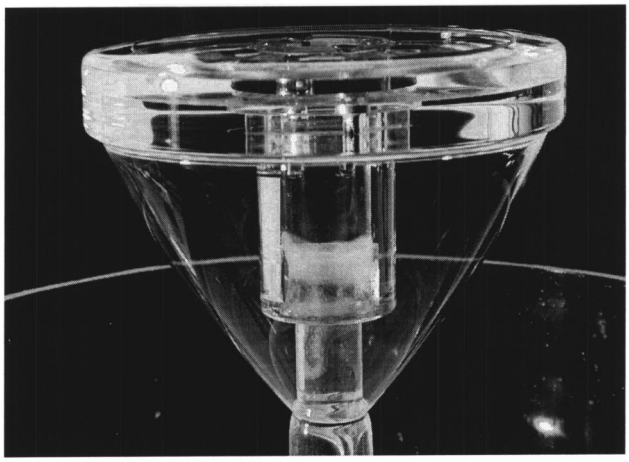

(a)

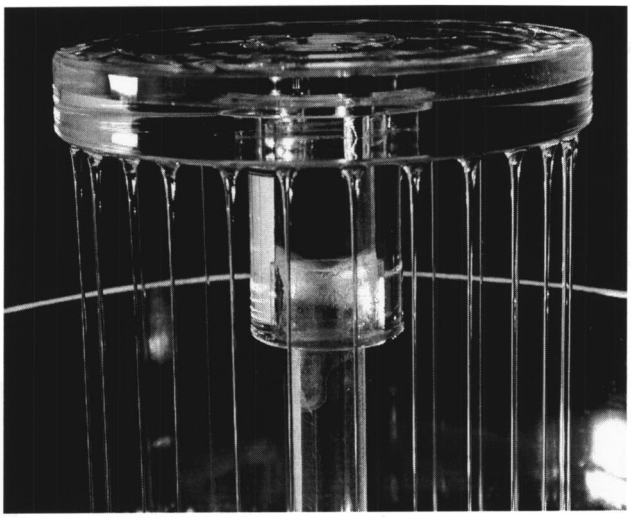

(b)

FIG. 3. (a) Viscous oil bell generated under an overflowing circular dish. (b) Array of liquid column obtained in the same conditions as (a) but lower flow rate.

In the present paper we investigate the shape and behavior of a particular kind of liquid bell that is in some sense intermediate between axisymmetrical sheets or bells obtained by jet impact and falling liquid curtains. An example of these so-called ''transonic liquid bells'' is presented in Fig. 3(a). In our experiment, such bells are formed below an overflowing dish supplied with liquid at constant rate when the flow over the dish is ''sufficient.'' At ''low'' flow rates, instead of the bell, one observes liquid columns, as presented in Fig. 3(b). This latter regime has motivated several studies,[19–22] especially since it provides a large variety of one-dimensional nonlinear dynamical patterns.[23,24] At higher

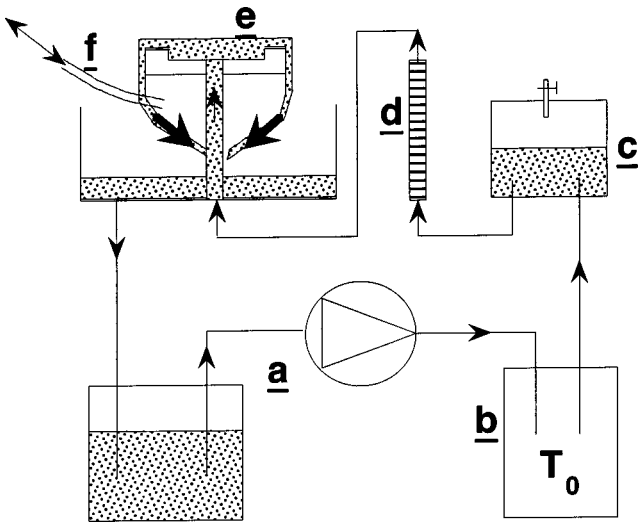

FIG. 4. Experimental setup.

flow rate, one observes a liquid bell such as that reproduced in Fig. 3(a), in which the vertical structure of the flow is very similar to that involved in a falling curtain (free fall), but with periodic boundary conditions that are reminiscent of more classical sheets and bells obtained by jet impact. In the context of curtain stability, this last point is very interesting since in most experiments involving liquid curtains,[11,15] it is necessary to guide the edges of the curtains to prevent shrinkage under the action of surface tension, these guides being potential sources of uncontrolled perturbations.

We present an exhaustive study of the shape of these liquid bells hanging below an overflowing dish, varying flow rate and internal pressure. In a way similar to a previous study performed on planar falling curtains by Finnicum *et al.*,[11] our experiment shows that an annular sheet with a large spatial region in which $We<1$ does not necessarily break. We do not address here the stability problem itself, but rather focus, for the present paper, on the shape of stable liquid bells obtained in these conditions with Newtonian viscous liquids. In particular, we emphasize the features induced by the presence of a transonic point on the shape calculations, and thus on the shape selection problem.

In Sec. II, we describe our experimental setup. In Sec. III, we present our experimental results, focusing on the structure of the flow and on the bell shapes. In Sec. IV, we recall the general equilibrium equations which govern the shape. In Sec. V, we solve these equations and compare the numerical shapes to those observed experimentally. In Sec. VI, we show that, close to the bursting limit, the bell can oscillate with three different modes (axial, planar, rotating) and we discuss qualitatively the observed frequencies.

II. EXPERIMENTAL SETUP

The setup is presented in Fig. 4: a liquid bell is formed below an overflowing circular dish (e), of radius R_0. We have used two different dishes with $R_0=5$ cm and $R_0=1.5$ cm. The flow is imposed by a gear pump Ismatec BVP *Z*, (a). The liquid is a silicon oil (poly-dimethyl siloxane, Rhodorsil 47V200), with dynamic viscosity $\mu=200.0(\pm1)$ cP, surface tension $\sigma=20.4$ dyn/cm, and density $\rho=0.97$ g/cm^3. This liquid is referred further by the abridged name ''V200.'' We must underline here that we were not able to obtain stable transonic bells with low viscosity liquids such as water: the liquid sheet always breaks. Experimentally, we have thus increased the liquid viscosity and observed that with a silicone oil 200 times more viscous than water, we were able to form a transonic stable bell. The fluid is injected at the dish center across a central hollow tube that supports the dish. Its temperature is kept constant by a thermostatic bath (b), Neslab RTE-101, and frequently measured during the experiment with a thermocouple in contact with the liquid arriving in the dish. We have kept it in the range (21, 22 °C). The half filled chamber (c), which consists in a cylinder of diameter 25 cm and height 10 cm, damps the possible noise of mechanical origin generated by the pump. A flow-meter (d) (Brooks full-view GT1024 size 8) allows to tune the flow rate. The liquid is then driven toward a cylinder, whose internal and external radii are respectively equal to 1.5 and 2.5 cm. It is possible to vary the internal pressure of the bell by injecting or removing air with a tube (f). The dish horizontality is tuned with the method exposed by Brunet *et al.*:[21] at a sufficiently low flow rate, the bell breaks and a circular array of liquid columns is formed instead of the bell. The liquid columns exhibit a collective dynamics that is very sensitive to the dish horizontality. For instance, in specific conditions (high enough column spacing increased by forcing coalescences), the column pattern undergoes a spatial period doubling in which the column positions oscillate, each one being out of phase with its two neighbors. The horizontality is nearly perfect when the oscillation amplitude is uniform around the dish. The bell is observed with a charge coupled device camera, images being captured and analyzed on a G3 Power PC Macintosh computer, across a Data Translation card, using NIH Image software. Except in Sec. VI, the side edge of the dish is steep [as presented in Fig. 5(a)]. This geometry imposes liquid detachment at the very edge of the dish, i.e., a bell radius (defined in a horizontal plane) $R(Z)$ equal to R_0 when $Z=0$. If the overhang is flat, as presented in Fig. 5(b), the flow is less constrained and the bell can select a different R for $Z=0$. In certain conditions, this can lead to oscillatory instabilities of the bell.

III. PRELIMINARY OBSERVATIONS

Starting from the liquid column array [Fig. 3(b)], the appearance of the liquid bell [Fig. 3(a)] requires a high enough flow rate. For the V200 silicon oil, and with a dish of radius $R_0=5$ cm, the bell replaces the circular array of liquid columns when the flow rate Q exceeds the critical value $Q_c=17.6$ cm^3/s, which corresponds to a flow rate per unit length of $\Gamma_c\equiv Q_c/2\pi R_0=0.587$ cm^2/s. The bell flow regime is strongly hysteretic: once the bell is formed, it is possible to reduce the flow rate to a very low value without bursting. The bursting flow rate Q_b is difficult to measure accurately: at a very low flow rate, the bell is very sensitive to perturbations, for instance the air flow in the experiment room. In this ''metastable'' regime, the bell walls are very thin and interference colors can be observed at the surface, which suggests

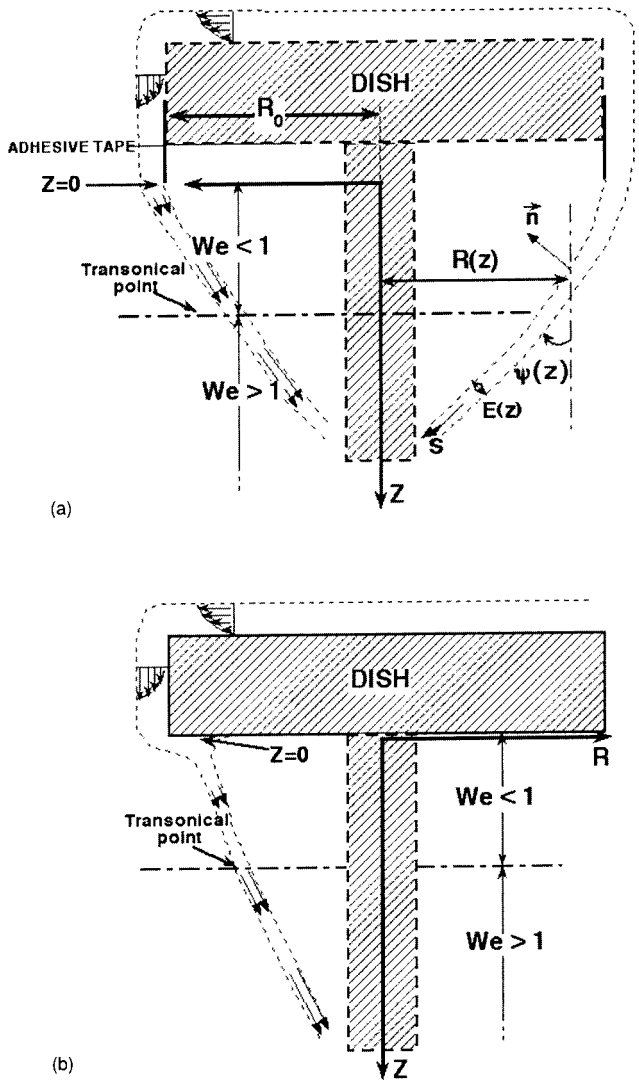

FIG. 5. (a) Qualitative structure of the flow, when the detachment is forced at the very edge of the dish with an adhesive tape rolled around the side on the dish. The bold dotted line suggests the expected free fall velocity flow profile that leads to a separation in two zones We>1 (stable) and We<1 (unstable). (b) Qualitative structure of the flow, when detachment is allowed everywhere below the dish.

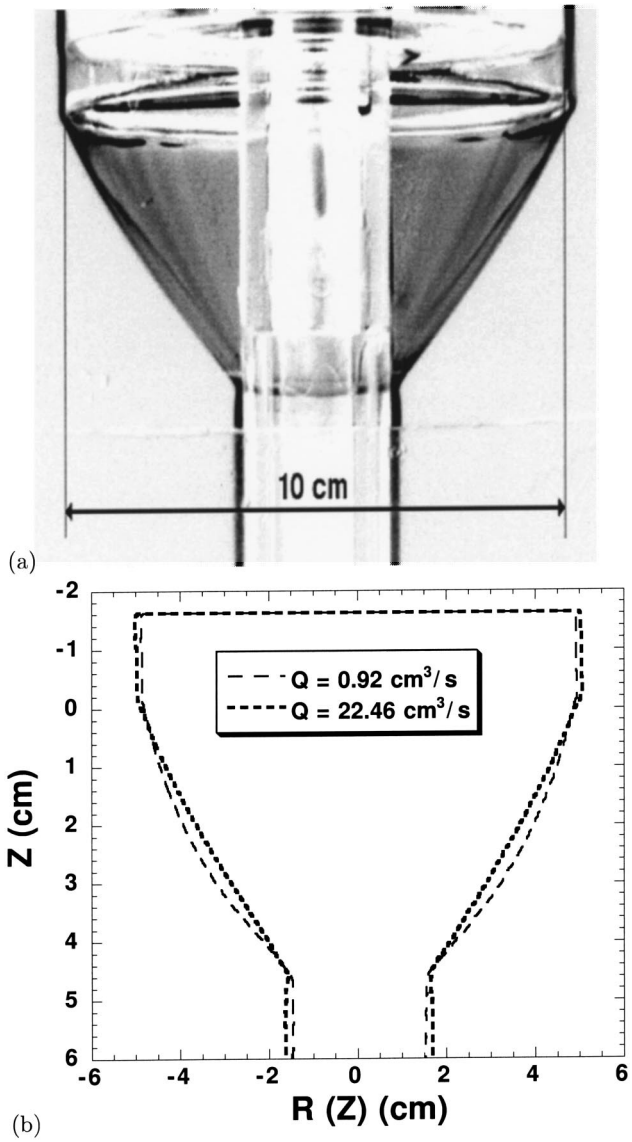

FIG. 6. (a) Picture of transonic bell obtained by substraction. The shape is then extracted, using a threshold. (b) Experimental shapes extracted for two extreme values of the flow rate with a noninflated bell. $Q=22.46\ \mathrm{cm}^3/\mathrm{s}$ and $Q=0.92\ \mathrm{cm}^3/\mathrm{s}$.

that holes are about to appear and to expand. As mentioned in Sec. II, a large viscosity appeared to improve the bell stability, and we chose therefore to work with a 200 cP silicon oil. In these conditions, the minimal flow rate allowed is of order $Q_b=0.855\ \mathrm{cm}^3/\mathrm{s}$, or $\Gamma_b=0.0285\ \mathrm{cm}^2/\mathrm{s}$. This is to be compared to the largest flow rate that we can reach with our gear pump of order $Q_M=25\ \mathrm{cm}^3/\mathrm{s}$ ($\Gamma_M=0.837\ \mathrm{cm}^2/\mathrm{s}$). The range of allowed flow rate for our study is large ($Q_M/Q_b\approx 30$).

Figure 6(a) shows the result of image subtraction between the side view of a bell and the same side view of the dry dish. By subtraction, we mainly see the liquid which appears as dark in the picture. Such treatment provides an easy way to measure the film thickness on the dish and to extract shapes such as those presented in Fig. 6(b). The two superposed profiles are obtained as follows: as soon as the bell is created, for high flow rates (approximately 22 cm^3/s for a dish radius of 5 cm), we extract the first shape. Then, the flow rate Q is strongly decreased: the bell remains stable until Q reaches a very small value around Q_b where we extract the second shape. Despite the reduction of the flow rate by a factor of 24, we observe that the difference between these two shapes is weak. Since the volume of air trapped inside the bell is constant, we deduce that the related variations of pressure are small. A very different behavior is observed with classical "water bells" formed by impingement of a jet on a solid surface: when one starts from a static closed bell, and decreases the flow rate, a bursting of the bell is observed leading to the birth of a new one with an internal pressure equal to the ambient value.[7] We have not observed such an instability with our transonic liquid bells.

Prior to the detailed analysis of the shape, we study the structure of the flow, and first start by the lubrication film on the side of the dish. For a given flow rate, it is observed that the liquid thickness on the side of the dish is constant [see

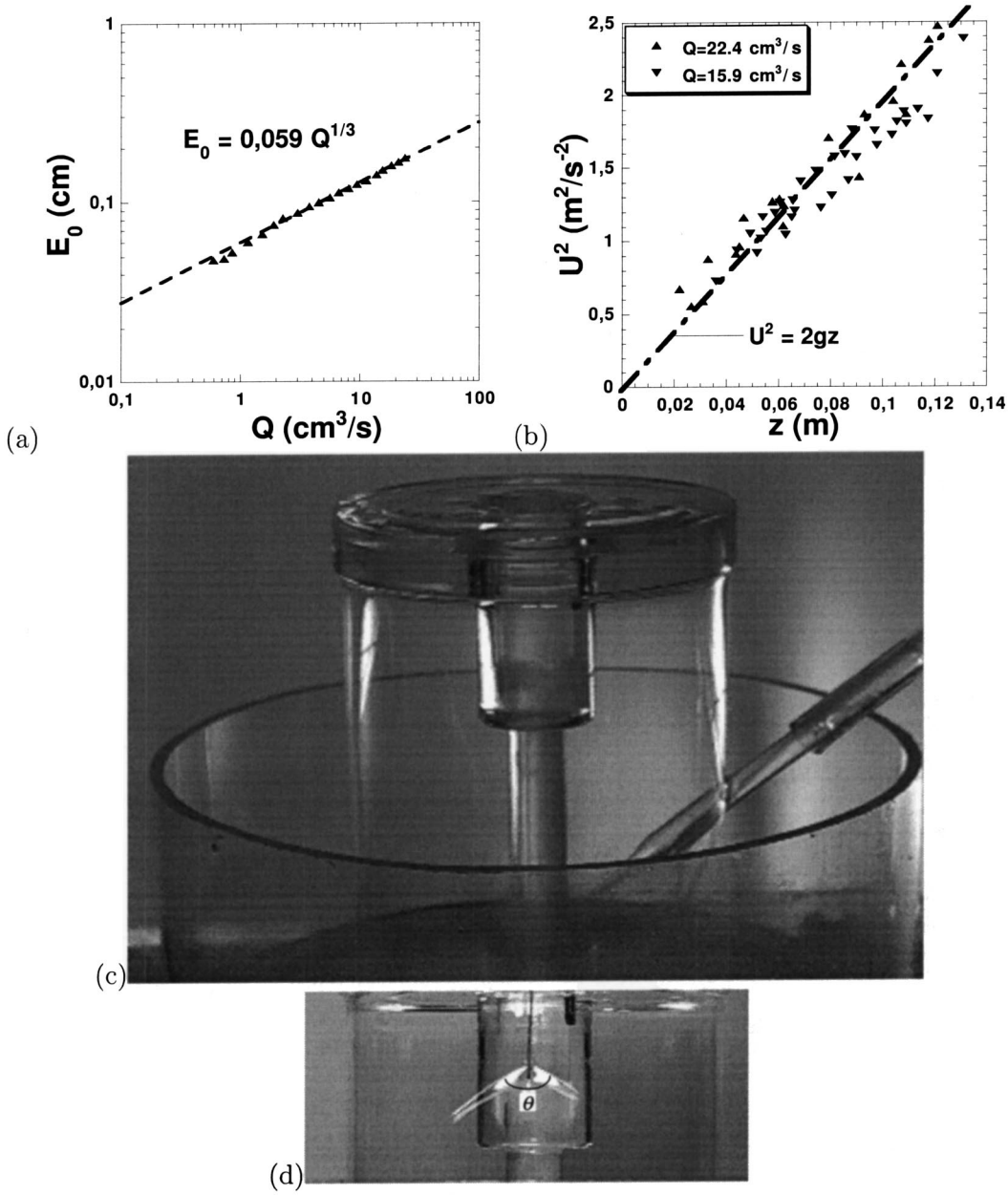

FIG. 7. (a) Liquid thickness at the side of the dish, vs flow rate (LOG–LOG plot). The fitting curve is an algebraic law, with a power 1/3. (b) Vertical velocity versus distance to dish, deduced by measurements on sinuous wakes behind a needle, for two values of the flow rate. Data suggest a free-fall law, added to an offset: $U^2 = U_0^2 + 2gZ$, U_0 depending on the flow rate but staying very small compared to $2gZ$. This result is obtained with both configurations of Figs. 5(a) and 5(b), but the line $z=0$ lies at two different places with or without the adhesive tape. (c) Cylindrical bell obtained by pumping a large volume of air inside. The measurements of velocity fields have been done with this situation.

Fig. 6(a)], so that inertia is negligible in this part of the flow. In these conditions, the lubrication theory predicts a thickness which takes the following expression:

$$E_0 = \left(\frac{3\mu}{2\pi R_0 \rho g}\right)^{1/3} Q^{1/3}. \tag{3}$$

The evolution of the film thickness with the flow rate has been checked and the results, obtained with $R_0 = 5$ cm, are presented in Fig. 7(a). In this figure, we observe that the experimental measurements are in close agreement with the solid line representing Eq. (3). Using the mass conservation, we can then deduce the mean velocity, U_0, in the film

$$U_0 = \left(\frac{\rho g}{12\mu\pi^2 R_0^2}\right)^{1/3} Q^{2/3}. \tag{4}$$

With the flow rates used in our experiments, U_0 varies from 0.1 to 0.8 cm/s.

The velocity in the falling film is measured using the following method: to simplify the geometry, we have inflated the bell (using tube f) to form a perfect vertical cylindrical-shaped bell [a vertical sheet with periodic boundary conditions, see Fig. 7(c)]. An obstacle (we used here a thin needle of diameter 0.5 mm) is put in the supersonic zone to create a

sinuous wake [Fig. 7(d)]. The ''Mach angle'' θ is directly connected to the local velocity by the relation[4]

$$U=\frac{1}{\sin^2(\theta/2)}\frac{4\pi\sigma R}{\rho Q}. \tag{5}$$

To insure that mass conservation is verified close to the overhang, we take $U(Z=0)=U_0$. Neglecting viscous effects, surface tension gradients and friction with the ambient air, the fluid velocity should be given by

$$U^2=U_0^2+2gZ, \tag{6}$$

where Z is the vertical coordinate defined in Fig. 5(a).

The results, reported in Fig. 7(b), show that Eq. (6) is a reasonable approximation.

The needle can also be used to investigate the response of the bell to perturbations. When it is moved upward and leaves the supersonic region by crossing the transonic point, the wake disappears. This allows a precise determination of the sonic point. A bit surprisingly, the bell does not break when we keep moving the needle in the subsonic region. Several attempts showed that it was possible to gently perturb the flow in the upper subsonic domain (We$<$1) without causing its destruction (even if We$<$1 everywhere on the bell). The bell is just ''shaken'' a bit during nearly 1 s, while the perturbation propagates upstream, reflects on the overhang and finally vanishes. This confirms some observations of Finnicum *et al.*[11] performed on planar sheets. Now, on the other hand, a strong perturbation (for example when a larger obstacle is violently put in contact with the bell) in the subsonic zone creates an expanding hole leading to the breakup of the bell.

IV. CALCULATIONS OF THE BELL SHAPE

The calculation of the shape of a liquid bell has first been achieved by Boussinesq[2] and reformulated by Taylor.[4] We first present the method and show how to adapt it to the specific conditions of transonic bells. The shape of a liquid bell is to be deduced from the force balance projected normally to the bell surface. In what follows, Z is the vertical distance from the bottom of the overhang [Figs. 5(a) and 5(b)], $R(Z)$ is the radial coordinate of the bell, $E(Z)$ is its local thickness, S is the curvilinear coordinate, and ψ is the angle between the bell and the Z axis [see Fig. 5(a)].

For a steady shape, the balance of forces on a unit surface element written along the normal, takes the form[4]

$$2\sigma\left[\frac{\cos(\psi)}{R}-\frac{d\psi}{dS}\right]+\rho gE\sin(\psi)=\Delta P-\frac{d\psi}{dS}\rho EU^2. \tag{7}$$

The first term on the left-hand side represents surface tension forces by unit surface: $\cos\psi/R$ and $d\psi/ds$ are, respectively, the axisymmetric and the meridian curvature. The factor 2 accounts for the two sides of the surface element. The second term on the left-hand side of Eq. (7) is the weight. Next term $\Delta P\equiv P_{\text{int}}-P_{\text{ext}}$ represents the effect of a pressure difference across the bell. For an open bell, this term is null. The last term is the centrifugal force.

In addition to this force balance, the mass conservation takes the form

$$Q=2\pi URE. \tag{8}$$

Using this expression in Eq. (7) we remove the thickness, E, and get

$$\frac{d\psi}{dS}\left(\frac{\rho QU}{4\pi\sigma}-R\right)+\cos\psi=\frac{\Delta P}{2\sigma}R-\frac{\rho gQ}{4\pi\sigma U}\sin\psi. \tag{9}$$

For open bells in the low gravity limit, the right-hand side of Eq. (9) is null and Boussinesq has shown that the equation admits a catenary for analytical solution.[2]

To discuss the shape of transonic liquid bells, we introduce the characteristic length R_0 and the characteristic velocity $\sqrt{2gR_0}$:

$$r=\frac{R}{R_0},\quad z=\frac{Z}{R_0},\quad s=\frac{S}{R_0},\quad u=\frac{U}{\sqrt{2gR_0}}.$$

One finally obtains the nondimensional equation describing the bell shape

$$(2\beta u-r)\frac{d\psi}{ds}+\cos\psi=\alpha r-\beta\frac{\sin\psi}{u}, \tag{10}$$

where α and β, respectively, stand for the dimensionless pressure and gravity

$$\alpha=\frac{\Delta PR_0}{2\sigma},$$

$$\beta=\frac{\rho Q\sqrt{g}}{4\pi\sigma\sqrt{2R_0}}.$$

As stated earlier, α can be turned to zero by connecting both sides of the bell. Concerning β, its value changes from $\beta\approx0.03$, obtained with the smallest flow rate, to $\beta\approx0.7$ corresponding to the largest one. The effect of gravity can thus not be neglected.

We identify in Eq. (10), four unknowns: u, r, ψ, and s. Equation (6) which can be presented as the evolution of the momentum in the direction tangent to the bell surface provides a second equation and a new unknown z:

$$u^2=u_0^2+z, \tag{11}$$

where $u_0^2=U_0^2/(2gR_0)$ and U_0 is defined in Eq. (4). Since $U_0\lesssim1\ \text{cm s}^{-1}$, we deduce the order of magnitude $u_0\sim10^{-4}$. u_0 is then negligible in Eq. (11) as soon as Z is typically larger than a millimeter.

Finally, the system is closed using the three geometrical relations

$$ds^2=dr^2+dz^2, \tag{12}$$

$$\cos\psi=\frac{dz}{ds}, \tag{13}$$

$$\sin\psi=\frac{dr}{ds}. \tag{14}$$

Considering open bells with small curvature, such as the one presented in Fig. 3(a), we considered the limit $\alpha=0$ and $d\psi/ds\ll1$. In this limit, Eq. (10) reduces to

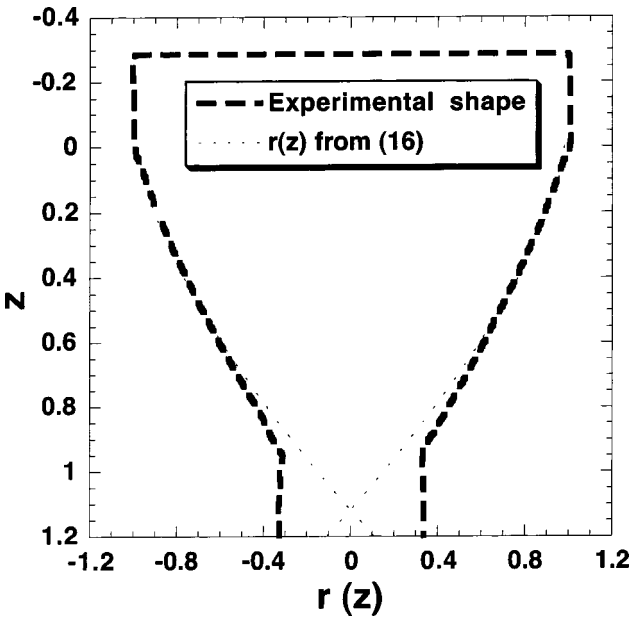

FIG. 8. Comparison between an experimental shape and the one obtained from Eq. (16), with a pressure difference equal to zero and $Q = 22.46\ \mathrm{cm}^3/\mathrm{s}$.

$$\tan\psi = -\frac{u}{\beta}, \tag{15}$$

which can be integrated using the geometrical relations and the boundary condition $r(z=0)=1$. The integration leads to the analytical expression of the shape

$$r(z) = 1 - \frac{2u_0^3}{3\beta}\left[\left(1+\frac{z}{u_0^2}\right)^{3/2} - 1\right]. \tag{16}$$

In Fig. 8, we compare this analytical solution to the shape observed experimentally with open bells ($\alpha=0$) and $Q = 22.46\ \mathrm{cm}^3\ \mathrm{s}^{-1}$. We observe that the analytical expression in dotted line is a good approximation of the actual shape.

In the general case, α is different from zero and the curvature cannot be neglected. The system of Eqs. (10)–(14) must then be integrated numerically.

V. NUMERICAL INTEGRATION OF THE SHAPE AND COMPARISON WITH EXPERIMENTS

Since $d\psi/ds$ is a second order derivative in $r(z)$, we need two boundary conditions to integrate the bell shape. The first condition is $r(z=0)=1$. The second condition is provided by the sonic point (the symbol * is used to designate the quantities obtained at the sonic point). $z=z^*$ where $2\beta u^* = r^*$. At this location, once z^* is known, u^* is deduced from Eq. (11), r^* from the condition $r^* = 2\beta u^*$ and ψ^* from Eq. (10):

$$\cos\psi^* = \alpha r^* - \beta\frac{\sin\psi^*}{u^*}.$$

Thus, if z^* is known, all the other quantities can be calculated. Numerically, we initially guess the position of $z^*>0$ and integrate the set of equations down to $z=0$ where the value of r is checked. The procedure is repeated until the first condition $r(z=0)=1$ is satisfied. Once z^* is found through this shooting method, the second part of the shape $z>z^*$, is computed and provides the entire shape.

The shapes obtained numerically using this procedure are compared to the shapes observed experimentally in Fig. 9. All of them have been obtained with $R_0 = 5$ cm. We first focus on Fig. 9(a), where there is no pressure jump across the bell ($\alpha=0$) and $Q = 22.46\ \mathrm{cm}^3\ \mathrm{s}^{-1}$. In this case, there is no parameter free and we observe no difference between the numerical shape and the actual one. The three other comparisons are conducted with a pressure difference ($\alpha\neq 0$) and the numerical calculation will be used to evaluate α, which is not measured in our experiment. Prior to comment on these values, we make several remarks on the numerical procedure used.

The necessity of the earlier algorithm can be understood considering Eq. (10). In this equation, the sonic point appears as the point where the coefficient of the higher derivative vanishes. It follows that a numerical integration cannot cross z^*. The crossing is thus avoided by starting the calculation at z^*, then going upward toward the dish to verify the other boundary condition and then finishing the calculation by the supersonic region.

Since the whole procedure depends on the existence of z^*, it is essential to show that this sonic point always exists in the bells we consider: this can be demonstrate by considering the respective evolution of r and $2\beta u$. When the film detaches from the dish, $r=1$ and $2\beta u_0$ is much smaller than unity. Since the bell is closed, r varies from 1 to 0. At the same time, u increases through the free fall law. There is thus a point where both quantities get equal: $r^* = 2\beta u^*$.

However in practice, for the lowest flow rates, the transonic point may disappear from the bell, due to the finite size of the central tube. In this case, the term $(r-2\beta u)$ is larger than zero everywhere. The corresponding bells do not exhibit a supersonic region and one do not observe any wake when moving the needle up and down along the whole surface of the bell. The different comparisons of shapes are performed with experimental bells which do exhibit a sonic point on their surface.

We now come back to the effect of a pressure difference on the shape of the bell. Experimentally, the bell is first formed with the flow rate Q_0 without any pressure difference, $\alpha=0$. (With our conditions, Q_0 has a minimal value close to 7.5 cm^3/s. At weaker flow rates, a bell cannot exist with a pressure difference equal to zero.) The flow rate is then changed to Q leading to a positive value of α if $Q < Q_0$ and to a negative one in the opposite case, $Q > Q_0$.

Numerically, we integrate the shape and select the α leading to the best comparison with the experimental bell.

In Fig. 9(b), the bell has first been formed with $Q_0 = 22.46\ \mathrm{cm}^3\ \mathrm{s}^{-1}$ and then compressed with $Q = 15.63\ \mathrm{cm}^3\ \mathrm{s}^{-1}$. The numerical shape presented with the solid line cannot be distinguished from the actual one. It is obtained with $\alpha=0.0466$, corresponding to a pressure difference $\Delta P \approx 0.38$ Pa. Such a small pressure difference can hardly be measured. This measure illustrate the extreme sensitivity of the bell shape to pressure difference, which make them almost perfect barometers.

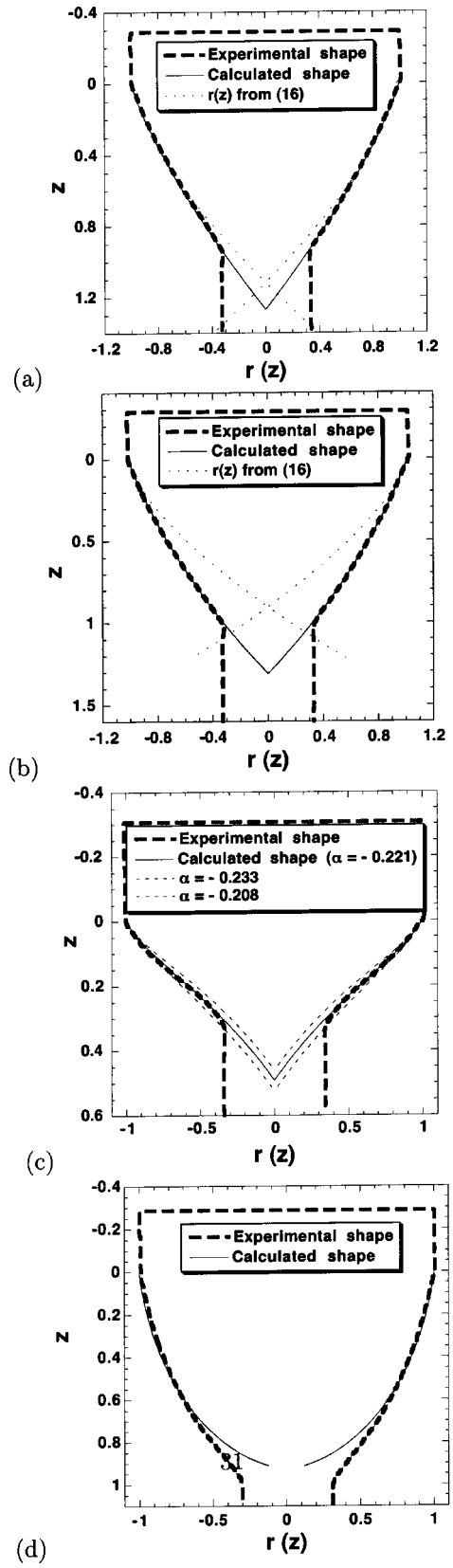

FIG. 9. (a) Experimental and calculated shapes for $Q=22.46\,\mathrm{cm}^3/\mathrm{s}$, $Q_0=22.46\,\mathrm{cm}^3/\mathrm{s}$, and $R=5$ cm. The nondimensional pressure α equals zero. The dotted curve represent the solution of Eq. (16). (b) Experimental and calculated shapes for $Q=15.63\,\mathrm{cm}^3/\mathrm{s}$, $Q_0=22.46\,\mathrm{cm}^3/\mathrm{s}$, and $R=5$ cm. The nondimensional pressure α is found equal to 0.0466 ($\Delta P=0.38$ Pa). (c) Same as (a) and (b) but with $Q=22.24\,\mathrm{cm}^3/\mathrm{s}$ and $Q_0=7.62\,\mathrm{cm}^3/\mathrm{s}$, leading to a strong depression inside the bell: $\alpha=-0.221$ ($\Delta P=-1.8$ Pa). (d) Same as (a) but with $Q=0.92\,\mathrm{cm}^3/\mathrm{s}$. α is found equal to 0.180 ($\Delta P=1.47$ Pa).

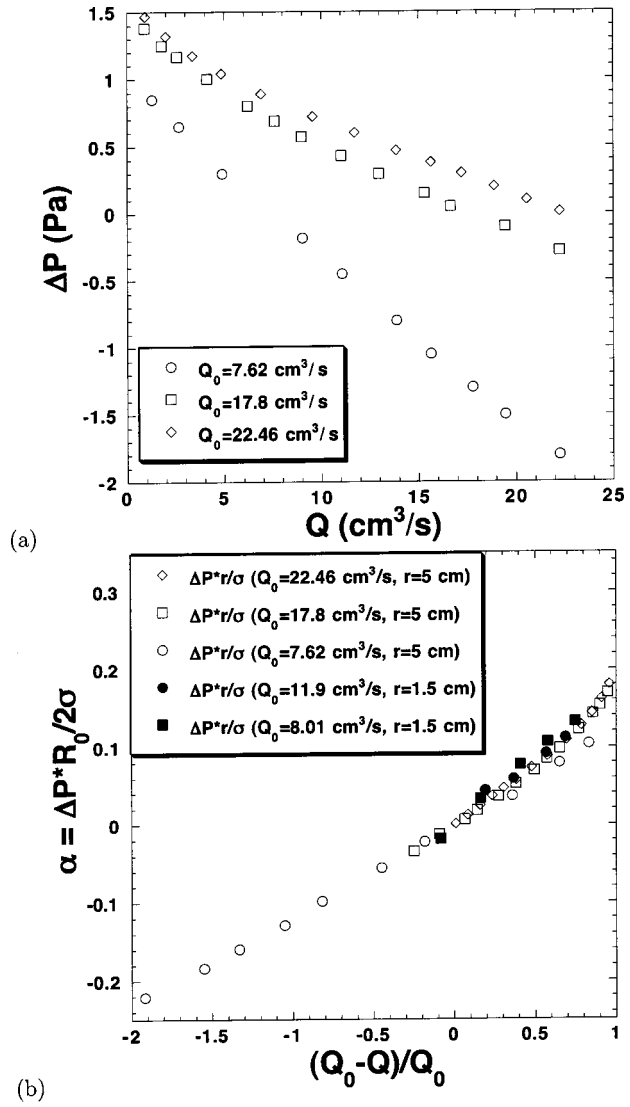

FIG. 10. (a) Open symbols: pressure difference vs flow rate for three values of Q_0 ($R=5$ cm). (b) Adimensional pressure α presented as a function of the nondimensional flow rate $(Q_0-Q)/Q_0$.

In Fig. 9(c), the bell is in depression: it is first formed with the flow rate $Q_0=7.62\,\mathrm{cm}^3\,\mathrm{s}^{-1}$ which is then increased to $Q=22.24\,\mathrm{cm}^3\,\mathrm{s}^{-1}$. The numerical shape presented in solid line superposes to the actual shape when $\alpha=-0.221$. This value corresponds to a depression of -1.8 Pa. To check the sensitivity of the shape on the free parameter α, we also present in Fig. 9(c), the shapes obtained with $\alpha=-0.233$ and $\alpha=-0.208$. These values differ from $\alpha=-0.221$ by $\pm 5\%$ and clearly do not superpose on the observed shape. Such comparisons lead us to estimate the uncertainty on α to be $\pm 2\%$.

Finally, in Fig. 9(d), we present the maximal compression, obtained with $Q_0=22.46\,\mathrm{cm}^3\,\mathrm{s}^{-1}$ and $Q=0.92\,\mathrm{cm}^3\,\mathrm{s}^{-1}$. Numerically, we measure $\alpha=0.18$, that is $\Delta P\approx 1.47$ Pa.

More generally, the relation between the pressure difference ΔP and the flow rate Q is presented in Fig. 10(a), for the same dish $R_0=5$ cm and different initial conditions Q_0. For a given Q_0 we observe that ΔP is a decreasing function

of Q. The order of magnitude is typically the Pascal. The same results are presented in a dimensionless form in Fig. 10(b), where α is plotted versus $(Q_0-Q)/Q_0$. We observe that all our measurements collapse on a single curve which can be approximated by the linear relation

$$\frac{\Delta P R_0}{2\sigma} \approx 0.1 \frac{Q_0-Q}{Q_0}. \tag{17}$$

This equation can be interpreted as the development of $\alpha \equiv \Delta P R_0/(2\sigma)$ in terms of $\epsilon \equiv (Q_0-Q)/Q_0$. As already discussed, α is null when the bell is open ($Q=Q_0$) and is changed when the bell is closed and the flow rate varied from its formation value ($Q \neq Q_0$). The general form of α can thus be written as $\alpha=\mathcal{F}(\epsilon)$, where the function $\mathcal{F}$ vanishes for $\epsilon=0$. We deduce that α can be expanded as

$$\alpha \approx \epsilon \mathcal{F}'(0) + \epsilon^2/2 \mathcal{F} \approx (0) + \ldots .$$

Equation (17) represents the leading order of this development from which we deduce $\mathcal{F}'(0) \approx 0.1$.

To conclude this section dedicated to the numerical integration of the bell shape, we present in Fig. 11, two others characteristic of the shape, namely, their volume [Fig. 11(a)] and the position of the sonic point z^* [Fig. 11(b)]. In Fig. 11(a), the volume of the numerical bell is shown to be independent of the flow rate Q and to increase with the initial condition Q_0. To be more precise, the volume perturbation $\Delta V/V_0$ should be of the order $-\Delta P/P_0 \lesssim 10^{-5}$ which is smaller than the accuracy of our calculation.

Concerning the position of the sonic point, we present in Fig. 11(b) its position relative to the maximal extension of the bell $z_{\max}$, for different values of the flow rate Q and different initial conditions Q_0. We observe that $z^*/z_{\max}$ is a decreasing function of Q and weakly depends on the initial condition Q_0. We also observe that $z^*/z_{\max}$ tends to one as Q approaches 0.

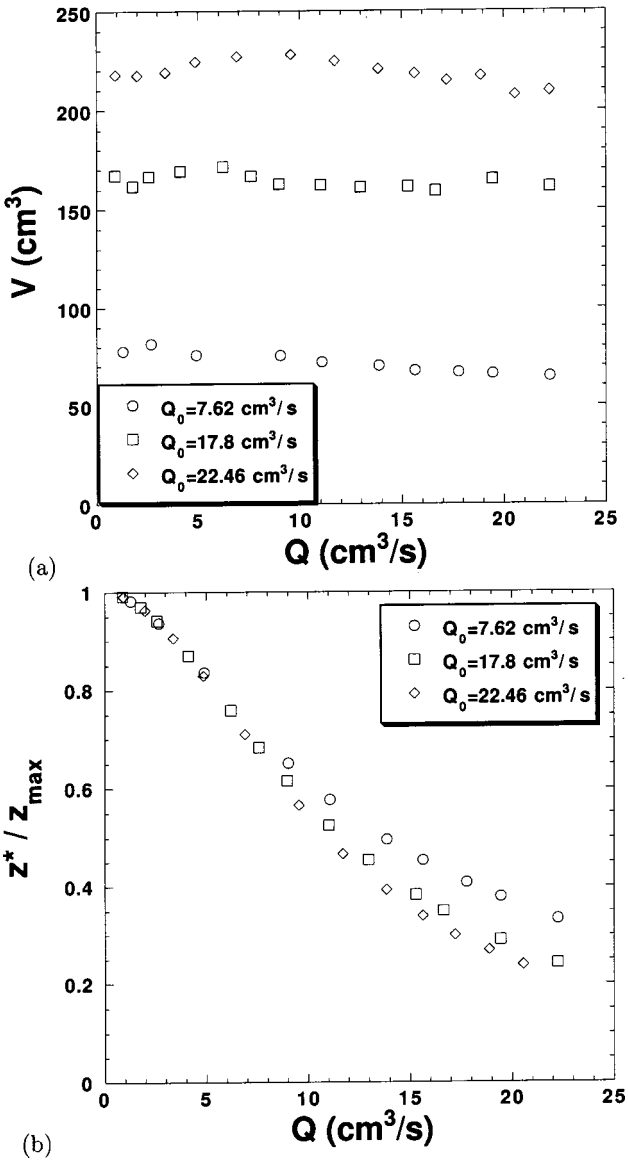

FIG. 11. (a) Volume of the bell vs flow rate, for three values of Q_0 ($R=5$ cm). (b) Relative position of the sonic point as a function of the flow rate, for three values of Q_0.

VI. TEAPOT EFFECT AND OSCILLATIONS

In this last section, we show that once the sonic point disappears from the bell surface (due to the presence of a central tube), the bell can oscillate with different modes. If the liquid overflows from a dish with an horizontal overhang, i.e., if the adhesive tape is removed from the edge of the dish [see Fig. 5(b)], different dynamical behaviors can be observed. The bell surface can oscillate as suggested on Fig. 12, this oscillation being coupled with modulations of the circle on which the bell intersects the solid ceiling (attachment perimeter).

It is to note here that, in this case (i.e., after removing the adhesive tape), the value of r at $z=0$ is no more imposed strictly at R_0, but can select a slightly smaller radius [as illustrated in Fig. 3(a)]. This is the consequence of the so-called teapot effect.[25]

Strictly speaking, we are not sure of the details involved in the physical mechanisms of these oscillations. The observed frequencies (see later) are close to those observed previously on liquid column arrays,[19–22] suggesting a possible coupling of instabilities of the film hanging below the ceiling and free horizontal motions of the bell walls.[19] Now, intuitively, we think that the disappearance of the sonic point plays also a central role here and we will insist on these aspects while presenting in more details our observations.

In this configuration (i.e., without adhesive tape), the solution of the shape can still be performed with the numerical method described in the previous section, except for the cases where the transonic point is taken away from the bell (at lowest flow rates). As the condition for $r(z=0)$ is not properly fixed and that no information from the transonic point is able to go upstream, the bell then ''hesitates'' between several possible shapes, corresponding to several possibilities for the angle $\psi(r=0)$. Actually, some dynamical modes start to grow preferentially, leading to oscillations. It is then remarkable that the emergence of these oscillations can be connected to the structure of the equation which governs the shape: this property can be seen as follows. Above the transonic point, the information can be driven upstream.

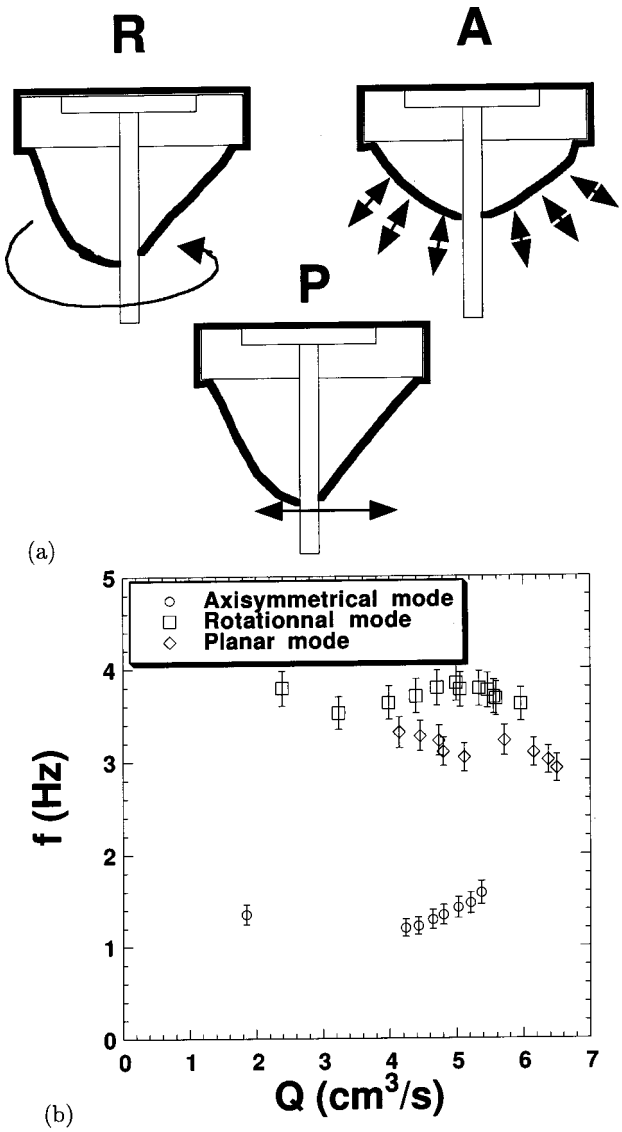

FIG. 12. (a) Oscillation modes developing on a liquid bell (dish without adhesive tape). Rotating (R), axisymmetric (A), and planar (P) oscillations. (b) Frequency of oscillations vs flow rate per unit length for the three previous modes.

If there is not any transonic point on the bell, the information given at this point, necessary to remove the singularity on the equations, cannot go upstream anymore.

These oscillations are about to last for a long time (more than 10 min), but they can lead to the bursting of the bell if their amplitude becomes too large. In order of magnitude, the amplitude of oscillations can vary from 1 mm to 2 or 3 cm. It is worth to notice that continuing to decrease flow rate, this amplitude decreases and oscillations disappear at very low flow rates (when $\Gamma<0.05$ cm^2/s).

Three main oscillation modes are observed [see Fig. 12(a)]. A rotating one (R), where the perturbation on $R(Z=0)$ turns around the dish, as a propagative wave. This perturbation is at the same time convected by the flow, showing a helicoidal-like motion for the bell. In the axisymmetric mode (A), the fluctuations of $R(Z=0)$ are simultaneously equal along the whole dish, as a stationary wave. The bell then has a motion comparable to the swimming of a Medusa. In the planar mode (P), perturbations on $R(R=0)$ are mainly localized in two diametrically opposite points. The resulting motion is a pendulum-like one, in a diametrical plan. This plan seems to be chosen by initial perturbations and it is about to slightly evolve in the same cycle of oscillations. It is possible to preferentially choose a mode rather than another, by pumping or deflating the bell, at the flow rate of its creation: an initially deflated bell, with a small volume and a large ejection angle preferentially generates axisymmetric oscillations. With a medium-sized bell, with an initial pressure difference nearly equal to zero, one observes both rotating and planar oscillations. A larger bell, initially pumped, most often generates planar oscillations. The largest bells, with a large internal pressure and which take a cylindrical shape do not exhibit oscillations. The reason is that, because of their height, these bells always include the transonic point (this has been experimentally observed, by creating a sinuous wake with a needle).

To measure the frequency of oscillations, and to verify more precisely than a direct view that these motions are periodic, oscillating bells are visualized by a camera put above the dish. A static bell appears as a dark circle which diameter is slightly smaller than the dish diameter. When the bell starts to oscillate, this circle is moving around its equilibrium position. By acquiring gray levels along the initial static circle, and creating spatiotemporal diagrams from these acquisitions, a clearly periodic phenomenon appears in the form of temporally regular dark lines (not reported) and a frequency can be precisely measured. The plot on Fig. 12(b) reports these measurements: no significant dependence with a flow rate has been noticed. Rotational oscillations have the higher frequencies (from 3.5 to 3.8 Hz). Planar oscillations have frequencies from 2.8 to 3.3 Hz. Axisymmetric ones are much slower: frequencies are from 1.2 to 1.6 Hz. It may be relevant to compare these frequencies to the one given by the frequency of vibration for a mass M with a sheet of tension 2σ. An order of magnitude for the frequency can be given by

$$f \simeq \frac{1}{2\pi}\sqrt{\frac{2\sigma}{M}}. \tag{18}$$

M is taken as the mass of air inside the bell added to the mass of liquid. The first term can be approximated by the mass of air inside a cone of base radius 5 cm and height 5 cm. The density of air equals 0.00129 g/cm^3 and the mass of air is near 0.2 g. The second term (mass of liquid sheet) can be deduced from the simple integration of $2\pi E(z)R(z)\rho$ (or $\rho Q/U(z)$ with the mass conservation [Eq. (8)] from $z=0$ to $z_{\max}$). One finds a value close to $\sqrt{2Q^2\rho^2 z_{\max}/g}$, which is approximately included from 0.1 to 0.5 g, in the range of flow rates where oscillations appears. σ is the surface tension of silicon oil (20 dyn/cm). The frequency f takes values from 1.2 to 1.8 Hz. This is close to the measurements obtained for the most symmetric mode of vibration [mode (A)]. The planar (P) and rotational (R) vibrations may correspond to higher modes (higher frequencies) because they are less symmetric than (A). Experimentally, the frequency is weakly in-

fluenced by the flow rate (and so, by the mass of the liquid), whereas Eq. (18) predicts a slight decrease of f with a flow rate.

VII. CONCLUSION

Usual water bells are obtained through the impact of a cylindrical jet on a solid disk of similar diameter. These bells form when the velocity of the jet overcomes the retraction speed of the rim, a condition which implies that the velocity in the liquid sheet is always larger than the speed of antisymmetrical waves. Usual water bells are thus said to be supersonic.

Here, we study the shape of transonic bells generated through the flow of a viscous liquid over a circular dish. The velocity of the liquid at the edge of the dish is much smaller than the velocity of antisymmetrical waves but becomes larger when leaving the dish, as it increases through a free fall law. The main property of these bells, is their ability to sustain a sonic point on their surface. Experimentally, this point can be precisely determined as the point above which the wake behind an obstacle disappears. We did not observe stable transonic bells with low viscosity liquids (the liquid sheet always broke) but with silicone oil 200 times more viscous. We do not report the study of the stability of the sheet but focus on their shape.

For ''open'' bells, we show that the shape mainly results from the equilibrium between gravity and surface tension. We derived in this limit an analytical solution for the shape.

In the general case, where there is a pressure jump across the bell, the shape must be integrated numerically. We then take advantage of the sonic point and integrate the equation from this specific location up to the origin of the bell, where its radius is imposed by the dish. The shapes obtained through this method are in perfect agreement with the experimental bells.

The numerical method is then used to measure the pressure difference across the bell. We show that the shape of the bell is sensitive to a pressure difference of the order of 0.1 Pa. This extreme sensitivity make them a perfect barometer.

Finally, using the imperfection of our experimental setup, we where able to show that once the sonic point disappears from the bell surface, due to the presence of a central tube, the bell can oscillate with different modes. These oscillations were observed using a flat overhang where the location of the film on the dish is not strictly imposed. The characteristic frequency of these modes is close to the frequency of a pulsating bubble.

ACKNOWLEDGMENTS

The authors would like to thank J.-M. Flesselles for helpful suggestions concerning the control and formation of bells in this experiment. They also thank both referees for their constructive suggestions.

[1] F. Savart, ''Mémoire sur le choc d'une veine liquide lancée contre un plan circulaire,'' Ann. Chim. **54**, 56 (1833).
[2] J. Boussinesq, ''Théorie des expériences de Savart, sur la forme que prend une veine liquide après s'etre choquée contre un plan circulaire,'' C. R. Acad. Sci., Paris **69**, 45 (1869); **69**, 128 (1869).
[3] F. L. Hopwood, ''Water bells,'' Proc. Phys. Soc. London, Sect. B **65**, 2 (1952).
[4] G. I. Taylor, ''The dynamics of thin sheets of fluids. I Water bells. II Waves on fluid sheets. III Disintegration of fluid sheets,'' Proc. R. Soc. London, Ser. A **253**, 289 (1959).
[5] G. N. Lance and R. L. Perry, ''Water bells,'' Proc. Phys. Soc. London, Sect. B **66**, 1067 (1953).
[6] R. Buckingham and J. W. M. Bush, ''Fluid polygons,'' Gallery of Fluid Motion, Phys. Fluids **13**, S10 (2001).
[7] C. Clanet, ''Dynamics and stability of water bells,'' J. Fluid Mech. **430**, 111 (2001); ''Stability of water bells generated by jet impacts on a disk,'' Phys. Rev. Lett. **85**, 5106 (2000).
[8] N. Dombrowski and R. P. Fraser, ''Photographic investigation into the disintegration of liquid sheets,'' Philos. Trans. R. Soc. London, Ser. A **247**, 101 (1954).
[9] C. Clanet and E. Villermaux, ''Life of a smooth liquid sheet,'' J. Fluid Mech. **462**, 307 (2002); E. Villermaux and C. Clanet, ''Life of a flapping liquid sheet,'' *ibid.* **462**, 341 (2002).
[10] G. Vich, C. Dumouchel, and M. Ledoux, ''Mechanism of disintegration of flat liquid sheets,'' Proc. ILASS-Europe'96 Lund, 1996, p. 121.
[11] D. S. Finnicum, S. J. Weinstein, and K. J. Ruschak, ''The effect of applied pressure on the shape of a two-dimensional liquid curtain falling under the influence of gravity,'' J. Fluid Mech. **255**, 647 (1993).
[12] K. Miyamoto and Y. Katagiri, ''Curtain coating,'' *Proceedings of European Coating Symposium (Strasbourg)* (Chapman and Hall, London, 1997), Vol. 11c, p. 463.
[13] H. Alfredson and D. Söderberg, ''Experimental and theoretical stability investigations of plane liquid jets,'' Eur. J. Mech. B/Fluids **17**, 689 (1998).
[14] S. P. Lin, ''Stability of a viscous liquid curtain,'' J. Fluid Mech. **104**, 111 (1981).
[15] S. P. Lin and G. Roberts, ''Waves in a viscous liquid curtain,'' J. Fluid Mech. **112**, 443 (1981).
[16] L. de Luca, ''Experimental investigation of the global instability of plane sheet flows,'' J. Fluid Mech. **399**, 355 (1999).
[17] F. Cullik, ''Comments on a ruptured soap film,'' J. Appl. Phys. **31**, 1128 (1960).
[18] D. R. Brown, ''A study of the behavior of a thin sheet of a moving liquid,'' J. Fluid Mech. **10**, 297 (1961).
[19] F. Giorgiutti and L. Limat, ''Solitary dilation waves in a circular array of liquid columns,'' Physica D **103**, 590 (1997).
[20] C. Counillon, L. Daudet, T. Podgorski, and L. Limat, ''Dynamics of a liquid column array under periodic boundary conditions,'' Phys. Rev. Lett. **80**, 2117 (1998).
[21] P. Brunet, J.-M. Flesselles, and L. Limat, ''Parity breaking in a one-dimensional pattern: A quantitative study with controled wavelength,'' Europhys. Lett. **56**, 221 (2001).
[22] P. Brunet, ''Structure et dynamique non-linéaire de liquides tombant,'' Thèse Université Paris, 2002, p. 6.
[23] J.-M. Flesselles, A. J. Simon, and A. J. Libchaber, ''Dynamics of one-dimensional interfaces: An experimentalist's view,'' Adv. Phys. **40**, 1 (1991).
[24] M. C. Cross and P. C. Hohenberg, ''Pattern formation outside of equilibrium,'' Rev. Mod. Phys. **65**, 851 (1993).
[25] S. F. Kistler and L. E. Scriven, ''The teapot effect: Sheet forming flows with deflection, wetting and hysteresis,'' J. Fluid Mech. **263**, 19 (1994).